J. Fluid Mech. (1967), *vol.* 27, *part* 2, *pp.* 315–336
Printed in Great Britain

Inviscid hypersonic flow over plane power-law bodies

By H. G. HORNUNG
Aeronautical Research Laboratories, Melbourne

(Received 22 December 1965 and in revised form 26 May 1966)

Theoretical solutions based on the expansion scheme for large x and large M_∞, as proposed by Freeman (1962), are obtained for the asymptotic inviscid flow over plane bodies of the shape $y/d = (x/d)^m$ in the range $\frac{2}{3}/\gamma < m < \frac{2}{3}$ where blast wave theory applies as a first approximation. In particular, the second-order terms, which are necessary to satisfy the body boundary conditions for the normal velocity are computed. The magnitude of the second-order terms is found to increase from zero at $m = \frac{2}{3}/\gamma$ to infinity at $m = \frac{2}{3}$.

As a comparison with theory, experiments at $M_\infty = 8{\cdot}2$ were made with two plane power-law bodies in the range $\frac{2}{3}/\gamma < m < \frac{2}{3}$ (at $m = \frac{1}{2}$ and $\frac{5}{8}$) and on a plane parabola with a tangent wedge nose. These consisted of the determination of shock-wave shapes, surface pressure distributions and detailed investigations of the distribution of pitot and static pressure across the shock layer.

The experimental results are in good agreement with the theory in the case $m = \frac{1}{2}$, where the second-order effects are small. At $m = \frac{5}{8}$ the region of validity of the theory is limited to much larger distances from the nose of the body and larger Mach numbers. Accordingly, the prediction for the deviation from first-order theory, although being correct in sign, is too small. Shock-wave shapes on bodies of the same power but of different size are correlated by the similarity theory when scaled with respect to the dimension d.

The experimental results obtained with the wedge-parabola are in very good agreement with a characteristics solution by C. H. Lewis (1965, unpublished).

1. Introduction

The theoretical part of this investigation is concerned with the inviscid, asymptotic flow field at large distances from the blunt nose of an asymptotically slender body when the free-stream Mach number is large and where the body still supports a strong shock wave. The appropriate equations of motion are simplified to the hypersonic small-disturbance equations developed by Hayes (1947), Goldsworthy (1952) and Van Dyke (1954). This simplification relies on the hypersonic similarity parameter $M_\infty \tau$ being finite with M_∞ large and τ small, where M_∞ is the free-stream Mach number and τ is a slenderness parameter. In deriving the hypersonic small-disturbance equations, terms of order τ^2 or M_∞^{-2} are neglected.

Under the assumption of a strong shock wave, these equations possess the self-similar solutions obtained by Lees & Kubota (1957), provided that the shock-wave shape is of the form $y_s \sim x^\mu$. The solutions have direct physical significance in the range $2/(3+j) < \mu \leqslant 1$, where $j = 0$ for plane flow and one for axisymmetric flow, the body being given by $y_b \sim x^m$ and here $m = \mu$. The solution for

$\mu = 2/(3+j)$ is singular since it does not satisfy the surface boundary condition. This singular solution corresponds to the solution of the one-dimensional unsteady problem of a constant-energy explosion obtained by Taylor (1950) and Sedov (1959) and has been interpreted by Lees (1955) and Cheng & Pallone (1956) as the solution appropriate for the blunt flat plate or cylinder. This interpretation is usually referred to as the 'blast-wave analogy'.

If the drag of a body for which the similar solutions apply is considered, the shock conditions give the pressure to be proportional to $x^{2(\mu-1)}$. Since similarity applies, the body pressure will also be proportional to $x^{2(\mu-1)}$. The body shape is $y \propto x^m$, and with $\mu = m$, the drag will be proportional to $\int x^{3(\mu-1)} x^{j\mu}\, dx$ which varies as const. $+ x^{(3+j)\mu-2}$. The constant can be interpreted as the drag of the blunt nose, the other term as the drag of the afterbody. For $\mu > 2/(3+j)$ it is seen that, for large x, the afterbody drag dominates, whereas for $\mu = 2/(3+j)$ the two terms are of equal order. Hence the drag of a body with $m < 2/(3+j)$ is finite and dominated by the effect of the blunt nose. This would suggest that the similar solution for $\mu = 2/(3+j)$ is a first approximation for the flow over all bodies in the range $0 < m < 2/(3+j)$. The effect of the asymptotic body variation then appears as a higher-order term.

The similarity solutions fail near the nose, where the small disturbance assumptions break down because of the blunt nose. It is possible however to treat the effect of the blunt nose as an upstream condition on the asymptotic flow by using the condition that entropy remains constant along streamlines. This upstream condition is not satisfied by the similar solutions in a layer near the body which has become known as the 'entropy layer' or 'cool core', because the entropy and temperature are required by the upstream condition to be lower than the predictions of the similar solutions.

Attempts to formulate a rational expansion procedure have been made by a number of authors, among them Guiraud (1958, 1964), Freeman (1962), Yakura (1962), Vaglio-Laurin (1964), Zolver (1964) and Messiter (1965). It will be sufficient for the purpose of this introduction to describe only a few of the results.

Yakura considered the 'inverse problem', in which the shock wave is given and the body shape is to be determined, and thus started with an entropy distribution which was known in terms of the stream function. This yielded an inner (entropy-layer) solution which could be joined by matching to an outer similar solution. Although the inverse approach removes many difficulties from the problem, it is open to criticism because, by choosing the shock-wave shape, one specifies the transition from the entropy layer to the outer solution and thus applies an artificial constraint to the system.

Guiraud (1958) considered the 'direct problem' for the case of the blunt flat plate or cylinder and obtained the order of magnitude of the error term introduced in the Sedov solution by the effect of the entropy layer.

Freeman (1962) considered the direct problem for power-law bodies in the range $0 < m < 1$ and obtained the order of magnitude of the error terms introduced in the respective first approximations in expansions in inverse powers of M_∞^2 for large x. He found that, in the range $0 < m < 2/(3+j)$, where the first approximation takes no account of the body shape, the error is due to the effect

of the body or entropy layer, depending on whether m is greater or less than $2/(3+j)\gamma$ respectively. In the range $2/(3+j) < m < 1$, the entropy layer was again found to give the important error, and only for $m > 2(\gamma+1)/\{(3+j)\gamma+2\}$ was the error term as small as that given by Van Dyke (1954) for slender bodies, and assumed by Yakura (1962), that is of order M_∞^{-2}. Figure 1 shows some of the results of this work in the form of a plot of error exponent versus m. The approach adopted here will be that used by Freeman and the analysis will be restricted to plane flow in the range $\frac{2}{3}/\gamma < m < \frac{2}{3}$, where the first approximation is the Sedov solution and the first perturbation is due to the body.

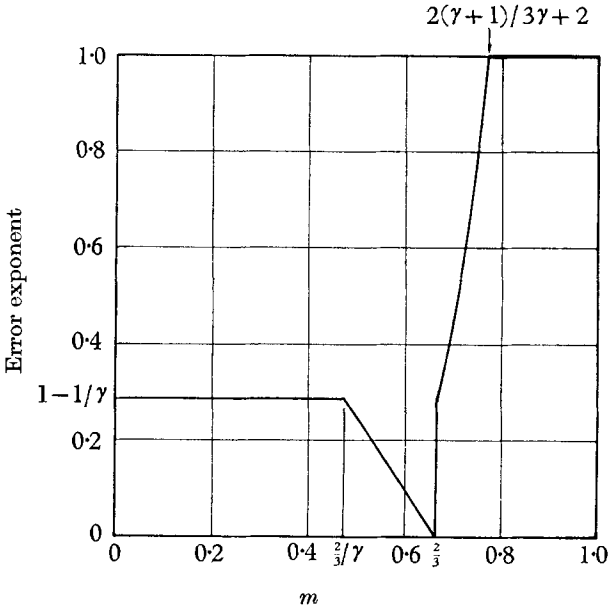

FIGURE 1. Order of magnitude of error of first-order theory, plotted as the exponent of M_∞^{-2} versus m, as obtained by Freeman (1962), $\gamma = 1{\cdot}4$.

Compared to the number of theories available for the blunt body problem, experimental data is limited. The most complete set of data is that of Kubota (1957) who obtained surface-pressure distributions, shock-wave shapes and Pitot-pressure traverses through the shock layer on three axisymmetric power-law bodies, $m = \frac{1}{2}$, $\frac{2}{3}$ and $\frac{3}{4}$ at $M_\infty = 7{\cdot}7$. All other available data are restricted to shock-wave shape and surface-pressure distribution, and very few deal with power-law bodies other than $m = 0$. Among them are the works of Hammitt & Bogdonoff (1956), Freeman, Cash & Bedder (1964) and Peckham (1965).

In order to determine the flow quantities in the shock layer from Pitot-pressure measurements alone, Kubota relied on the assumptions that the total temperature is constant and that the streamline slope is independent of the distance normal to the body. Although the second assumption becomes more and more accurate as $m \to 1$, it is certainly not satisfactory for $m < 2/(3+j)$, especially for the plane case. One would therefore like to measure additional quantities in order to avoid making this assumption and, if possible, to achieve some redundancy in the measurements to serve as a check.

2. Theory for $M_\infty \to \infty$

Derivation of differential equations

In accordance with the small-disturbance assumptions, it is appropriate to choose the following set of dimensionless variables:

$$\left.\begin{aligned} \text{pressure} \quad & p' = p/\rho_\infty a_\infty^2, \\ \text{density} \quad & \rho' = \rho/\rho_\infty, \\ x\text{-velocity} \quad & u' = \{(u/U_\infty) - 1\}/\delta, \\ y\text{-velocity} \quad & v' = v/a_\infty, \\ & y'/x' = y/x\sqrt{\delta}, \end{aligned}\right\} \tag{1}$$

where x, y are Cartesian co-ordinates, $\delta = M_\infty^{-2}$ and a_∞ is the free-stream sound speed. If the primed variables are defined as of order one, and terms of order δ are neglected, the equations of motion become the hypersonic small-disturbance equations:

$$\left.\begin{aligned} \frac{\partial u'}{\partial x'} + v' \frac{\partial u'}{\partial y'} + \frac{1}{\rho'} \frac{\partial p'}{\partial x'} &= 0, \\ \frac{\partial v'}{\partial x'} + v' \frac{\partial v'}{\partial y'} + \frac{1}{\rho'} \frac{\partial p'}{\partial y'} &= 0, \\ \frac{\partial}{\partial x'}(\rho' y'^j) + \frac{\partial}{\partial y'}(\rho' y'^j v') &= 0, \\ \left(\frac{\partial}{\partial x'} + v' \frac{\partial}{\partial y'}\right) \frac{p'}{\rho'^\gamma} &= 0, \end{aligned}\right\} \tag{2}$$

where γ is the ratio of specific heats.

The boundary conditions on the shock wave on which

$$\frac{dy'}{dx'} = \tan \phi',$$

become

$$\left.\begin{aligned} p' &= \frac{2}{\gamma+1} \tan^2 \phi' \left(1 - \frac{\gamma-1}{2\gamma} \cot^2 \phi'\right), \\ \rho' &= \left(\frac{\gamma-1}{\gamma+1} + \frac{2}{\gamma+1} \cot^2 \phi'\right)^{-1}, \\ u' &= \frac{2}{\gamma+1} \tan^2 \phi' (1 - \cot^2 \phi'), \\ v' &= \frac{2}{\gamma+1} \tan \phi' (1 - \cot^2 \phi'). \end{aligned}\right\} \tag{3a}$$

The boundary condition on the body which requires the body surface to be a streamline is

$$v' = dy'/dx' \quad \text{on} \quad y' = y_b'. \tag{3b}$$

The equation and boundary condition for u' are not coupled with the remaining equations and need not be considered in a solution for p', ρ' and v'. For the case of a strong shock wave, $\tan^2 \phi'$ is large, and the $\cot^2 \phi'$ terms in (3a) may be neglected.

The equations can now be written in terms of a similarity variable $\eta = \psi'/\psi'_s$, where the stream function ψ' is defined by

$$\partial\psi'/\partial y' = \rho' y'^j, \quad \partial\psi'/\partial x' = -\rho' y'^j v',$$

and

$$\psi'_s = y'^{j+1}_s = \{C_0 x'^{2/(3+j)}\}^{j+1}$$

is the value of ψ' on the shock wave. Considering the plane case, $j = 0$, for $m < \frac{2}{3}$, equations (2) become

$$\left.\begin{aligned} \frac{\partial v'}{\partial x'} - \frac{\frac{2}{3}\eta}{x'}\frac{\partial v'}{\partial \eta} + \frac{1}{x'^{\frac{2}{3}}}\frac{\partial p'}{\partial \eta} &= 0, \\ \left(\frac{\partial}{\partial x'} - \frac{\frac{2}{3}\eta}{x'}\frac{\partial}{\partial \eta}\right)\frac{p'}{\rho'^\gamma} &= 0, \\ \frac{\partial \rho'}{\partial x'} - \frac{\frac{2}{3}\eta}{x'}\frac{\partial \rho'}{\partial \eta} + \frac{\rho'^2}{x'^{\frac{2}{3}}}\frac{\partial v'}{\partial \eta} &= 0. \end{aligned}\right\} \tag{4}$$

The effect of a power-law body of the form $y/d = (x/d)^m$, where $\frac{2}{3}/\gamma < m < \frac{2}{3}$, can now be incorporated in an expansion for the flow variables in the outer region as follows (see Freeman 1962):

$$y'_s = C_0 x'^{\frac{2}{3}} + C_1 \delta^{1-\frac{3}{2}m} x'^m + \ldots, \tag{5}$$

$$\left.\begin{aligned} p' &= C_0^2 x'^{-\frac{2}{3}} P_0(\eta) + \delta^{1-\frac{3}{2}m} x'^{m-\frac{4}{3}} C_0 C_1 P_1(\eta) + \ldots, \\ v' &= C_0 x'^{-\frac{1}{3}} V_0(\eta) + \delta^{1-\frac{3}{2}m} x'^{m-1} C_1 V_1(\eta) + \ldots, \\ \rho' &= R_0(\eta) + \delta^{1-\frac{3}{2}m} x'^{m-\frac{2}{3}} (C_1/C_0) R_1(\eta) + \ldots, \\ y' &= C_0 x'^{\frac{2}{3}} Y_0(\eta) + \delta^{1-\frac{3}{2}m} x'^m C_1 Y_1(\eta) + \ldots. \end{aligned}\right\} \tag{6}$$

The first-order terms in these expansions represent the blast-wave approximation. The coefficients C_0 and C_1 are functions of m and γ and are to be determined later. If C_0 is to be of order one, the ratio of the scales for the primed co-ordinates in (1) requires that the body shape in primed co-ordinates be given by

$$y'_b = x'^m \delta^{1-\frac{3}{2}m}.$$

This determines the magnitude of the perturbations introduced by the body in the outer expansions (6). Substituting the expansions (6) into equations (4), and collecting terms of equal order in δ, the first- and second-order equations are independent of x':

$$\left.\begin{aligned} \frac{dP_0}{d\eta} - \tfrac{1}{3}V_0 - \tfrac{2}{3}\eta\frac{dV_0}{d\eta} &= 0, \\ \frac{P_0}{R_0^\gamma} &= \frac{8}{9(\gamma+1)}\left(\frac{\gamma-1}{\gamma+1}\right)^\gamma \frac{1}{\eta}, \\ \tfrac{2}{3}\eta\frac{dR_0}{d\eta} - R_0^2\frac{dV_0}{d\eta} &= 0, \\ R_0\frac{dY_0}{d\eta} &= 1, \end{aligned}\right\} \tag{7}$$

$$\left.\begin{aligned} \frac{dP_1}{d\eta} - (1-m)V_1 - \tfrac{2}{3}\eta\frac{dV_1}{d\eta} &= 0, \\ \frac{P_1}{P_0} - \gamma\frac{R_1}{R_0} &= \frac{3m}{\eta^{1-\frac{3}{2}m}}, \\ R_0^2\frac{dV_1}{d\eta} - \tfrac{2}{3}\eta\frac{dR_1}{d\eta} - \left(\tfrac{2}{3} - m - 2R_0\frac{dV_0}{d\eta}\right)R_1 &= 0, \\ R_0^2\frac{dY_1}{d\eta} + R_1 &= 0. \end{aligned}\right\} \tag{8}$$

The equation for the conservation of entropy along streamlines has been integrated in equations (7) and (8) using the shock-wave shape, equation (5). The equations for Y_0 and Y_1 result from the definition of the stream function.

The similarity variable η is taken equal to one on the first-order shock wave, $y' = C_0 x'^{\frac{2}{3}}$. The strong form of the shock-wave boundary conditions must be applied at the new location of the shock. It is convenient to expand these boundary conditions as a Taylor series in $(\eta_s - 1)$ such that the second-order boundary conditions can be given on $\eta = 1$ in terms of first-order derivatives. The boundary conditions are then obtained as:

$$\left.\begin{aligned} P_0(1) &= 8/9(\gamma+1), \quad V_0(1) = 4/3(\gamma+1), \\ R_0(1) &= (\gamma+1)/(\gamma-1), \quad Y_0(1) = 1, \end{aligned}\right\} \tag{9}$$

and

$$\left.\begin{aligned} P_1(1) &= \frac{8m}{3(\gamma+1)} - \left(\frac{dP_0}{d\eta}\right)_{\eta=1}, \quad R_1(1) = -\left(\frac{dR_0}{d\eta}\right)_{\eta=1}, \\ V_1(1) &= \frac{2m}{\gamma+1} - \left(\frac{dV_0}{d\eta}\right)_{\eta=1}, \quad V_1(0) = \frac{m}{C_1}, \\ Y_1(1) &= 1 - \left(\frac{dY_0}{d\eta}\right)_{\eta=1}, \quad Y_1(0) = \frac{1}{C_1}. \end{aligned}\right\} \tag{10}$$

The equations can be solved without considering the equations and boundary conditions for Y_0 and Y_1. Furthermore, since the second of equations (7) and the second of equations (8) have already been integrated using the shock conditions for P_0, R_0, P_1 and R_1, the boundary conditions for P_0 and P_1 cannot be used again. There remain five boundary conditions, one of which—$V_1(0) = m/C_1$—serves to determine the unknown coefficient C_1 which is common to all the perturbation quantities. The boundary condition for $Y_1(0)$ also gives C_1, but this is not an independent condition. It merely leads to the identity $Y_1(0) = (1/m)V_1(0)$. This is a useful check in the numerical calculations.

Series solution for small η and matching with entropy layer

The solution for the first-order equations, which has been given by Sedov (1959) analytically, has the following behaviour for small η:

$$\left.\begin{aligned} p' &= C_0^2 x'^{-\frac{2}{3}} P_0(0), \\ v' &= C_0 x'^{-\frac{1}{3}} \frac{2}{3(\gamma+1)}\left(\frac{8}{9(\gamma+1)P_0(0)}\right)^{1/\gamma}\eta^{1-1/\gamma}, \\ \rho' &= \frac{\gamma+1}{\gamma-1}[\tfrac{9}{8}(\gamma+1)P_0(0)]^{1/\gamma}\eta^{1/\gamma}. \end{aligned}\right\} \tag{11}$$

Substituting these expressions in equations (8) the coefficients become known functions of η. The resulting equations have the following solutions for small η:

$$\left.\begin{aligned} P_1 &= P_1(0) - (1-m)V_1(0)\eta + \frac{2m(1-\frac{2}{3}/\gamma)}{A\gamma^2(\frac{3}{2}m-1/\gamma)}\,\frac{\eta^{\frac{3}{2}m-(1/\gamma)+1}}{\frac{3}{2}m-(1/\gamma)+1} + O(\eta^{2-1/\gamma}),\\ V_1 &= V_1(0) + \frac{2m}{A\gamma^2}\,\frac{\eta^{\frac{3}{2}m-1/\gamma}}{\frac{3}{2}m-1/\gamma} - \frac{\frac{2}{3}/\gamma+m-\frac{2}{3}}{A\gamma(\gamma-1)}\,\frac{P_1(0)}{P_0(0)}\,\eta^{1-1/\gamma} + O(\eta^{\frac{3}{2}m-(2/\gamma)+2}),\\ R_1 &= -\frac{A}{\gamma}\,\eta^{1/\gamma}\left(\frac{P_1(0)}{P_0(0)} - 3m\eta^{\frac{3}{2}m-1}\right) + O(\eta^{1+1/\gamma}), \end{aligned}\right\} \quad (12)$$

where

$$A = \frac{\gamma+1}{\gamma-1}\,[\tfrac{9}{8}(\gamma+1)\,P_0(0)]^{1/\gamma}.$$

As is to be expected, these solutions fail at $m = \frac{2}{3}/\gamma$, and $m = \frac{2}{3}$. At both values the series are characterized by the confluence of exponents of η, and thus by the appearance of logarithmic terms.

The difficulty associated with these logarithmic terms lies in the matching of this solution with the solution in the entropy layer. In this region a solution can be obtained using the conservation of entropy along a streamline close to the body from the point where the streamline crosses the nearly normal shock wave. It is necessary to relax the small disturbance assumptions for this purpose, such that

$$p_s = \frac{2}{\gamma+1}\,\frac{1}{1+\cot^2\phi}.$$

Such a procedure gives the behaviour of the density and normal distance at the outer edge of the entropy layer. These inner solutions are matched with the outer solutions to the second order so long as m is not equal to $\frac{2}{3}/\gamma$ or $\frac{2}{3}$. At $m = \frac{2}{3}/\gamma$ the difficulty lies in the matching of the logarithmic term.

The problem for $m = 0$ is characterized by a perturbation of the shock-wave shape of the form $\delta^{1-1/\gamma}x'^{\frac{2}{3}/\gamma}$ in the analysis of Freeman (1962). This will always lead to the difficulty encountered in the above case $m = \frac{2}{3}/\gamma$, that the logarithm cannot be matched. Guiraud (1964) and Messiter (1965) avoid this difficulty by disallowing a shock-wave perturbation of this form and considering the next perturbation to be of the form $\delta^{2(1-1/\gamma)}x'^{(\frac{4}{3}/\gamma)-\frac{2}{3}}$. Although this allows the entropy layer to be matched with the outer solution when $m = 0$, it does not remove the difficulty when $m = \frac{2}{3}/\gamma$, since then a perturbation of the form $\delta^{1-1/\gamma}x'^{\frac{2}{3}/\gamma}$ appears from the body. The reason for the failure of the matching procedure when $m = \frac{2}{3}/\gamma$ is not obvious, but it is probable that similarity solutions of this type are then not available.†

Energy considerations and numerical solution

By considering an energy balance of the flow it has been shown by various authors that

$$C_0\int_0^{\eta_s}\left(\frac{p'}{(\gamma-1)\rho'} + \tfrac{1}{2}v'^2\right)d\eta = \int_0^{x'}(p'v')_{\eta=0}\,dx' = D_x/\rho_\infty U_\infty^2 d, \quad (13)$$

† One of the referees of this paper has drawn my attention to a more recent publication by Guiraud, Vallée & Zolver (1965) which goes into the problem $m = 0$ in more detail. It also presents a study of the relation between the direct and inverse approaches and a discussion of the basis of asymptotic hypersonic flows.

where D_x is the drag to x of the body. (See Kubota 1957; Freeman 1962; Guiraud 1964.) Substituting the expansions (6) in (13) and collecting terms of equal order in δ, the following results are obtained.

$$C_0^3 I_0 = D_\infty/\rho_\infty U_\infty^2 d, \tag{14}$$

$$C_1\left(I_1+\tfrac{1}{2}V_0^2(1)+\frac{1}{\gamma-1}\frac{P_0(1)}{R_0(1)}\right) = -\frac{m}{\frac{2}{3}-m}P_0(0), \tag{15}$$

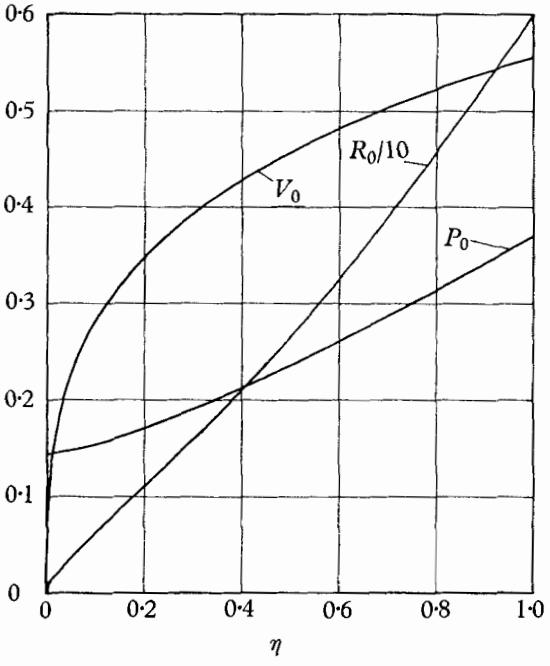

FIGURE 2. Solution of equations (7). First-order quantities, $m < \frac{2}{3}$, $\gamma = 1{\cdot}4$.

where, for $\gamma = 1{\cdot}4$,

$$I_0 = \int_0^1 \left(\frac{P_0}{(\gamma-1)R_0}+\tfrac{1}{2}V_0^2\right)d\eta = 0{\cdot}5388,$$

$$I_1(m) = \int_0^1 \left\{V_1V_0+\frac{1}{\gamma-1}\left(\frac{P_1}{R_0}-\frac{P_0R_1}{R_0^2}\right)\right\}d\eta,$$

and D_∞ = drag to $x' = \infty$.

While (15) provides yet another means of checking the value of C_1, the constant C_0 cannot be obtained from (14) without the knowledge of D_∞. This can only be obtained from the pressure distribution on the nose of the body, which is outside the region of validity of the present theory. The asymptotic approach is thus unable to determine the magnitude of the first-order quantities.

Equations (7) and (8) were solved numerically on the London University Mercury Computer for 9 values of m in the range $\frac{2}{3}/\gamma < m < \frac{2}{3}$ when $\gamma = \frac{7}{5}$. The integrals I_0 and I_1 were also evaluated and the results are presented in figures 2–6. Figure 2 shows the solution of the first-order equations in the form $P_0(\eta)$, $R_0(\eta)$ and $V_0(\eta)$. The inadequacy of these near the body ($\eta = 0$) is

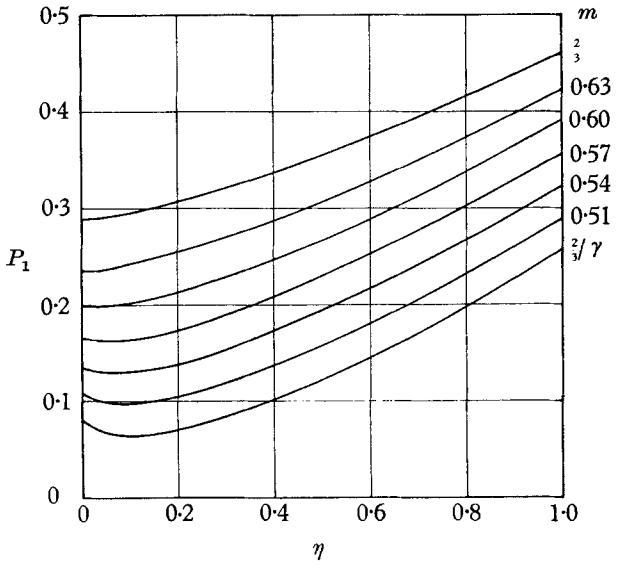

FIGURE 3. Solution of equations (8) for $P_1(m, \eta)$. Second-order pressure, $\gamma = 1{\cdot}4$.

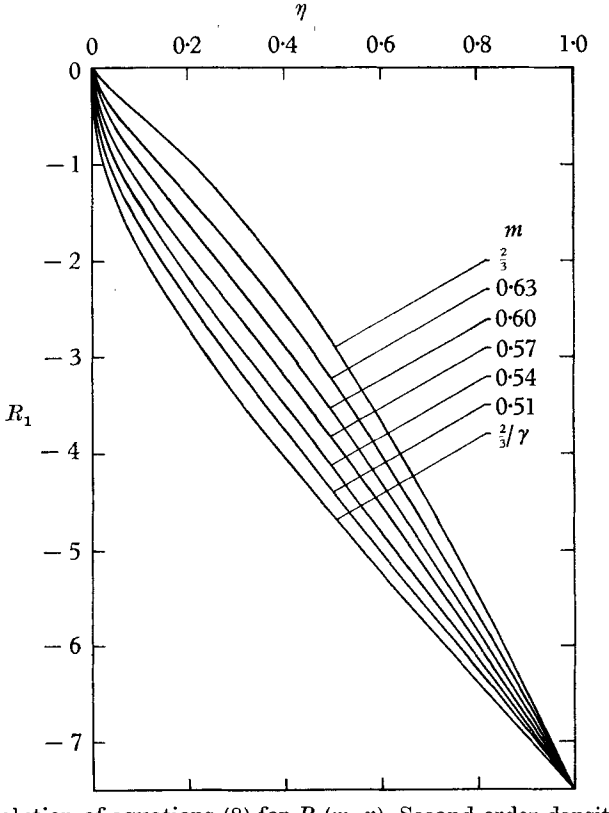

FIGURE 4. Solution of equations (8) for $R_1(m, \eta)$. Second-order density, $\gamma = 1{\cdot}4$.

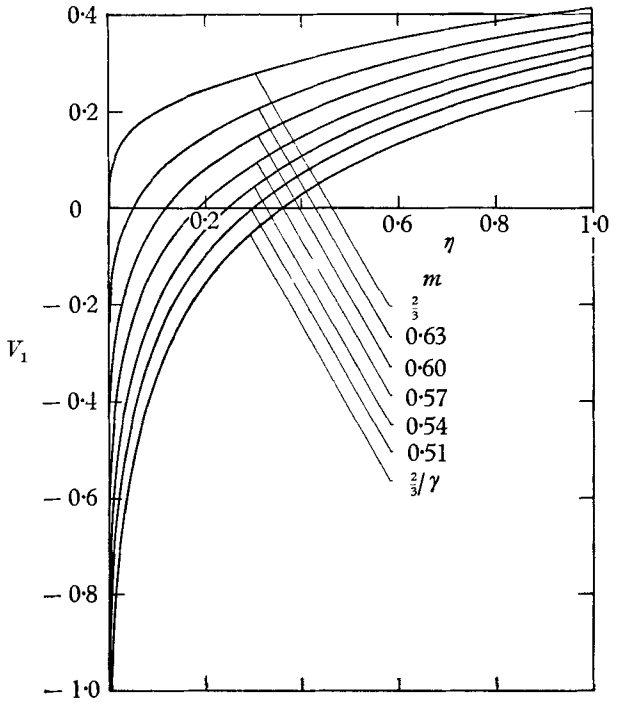

FIGURE 5. Solution of equations (8) for $V_1(m, \eta)$. Second-order normal velocity, $\gamma = 1{\cdot}4$.

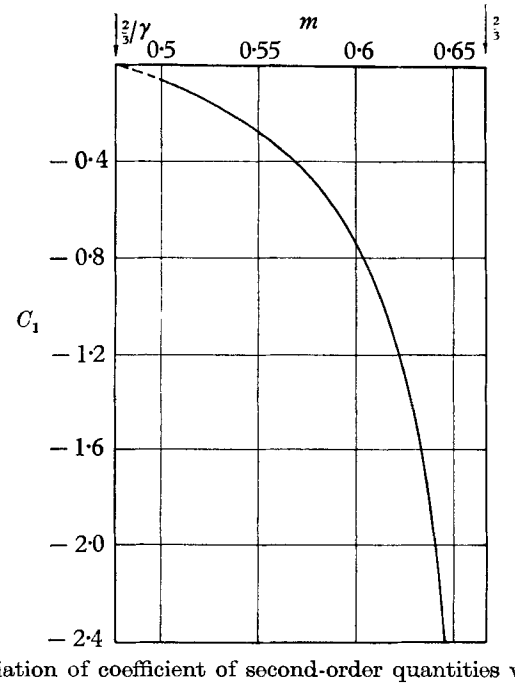

FIGURE 6. Variation of coefficient of second-order quantities with m, $\gamma = 1{\cdot}4$.

evident from the zeros of R_0 and V_0. Figures 3–5 give the second-order solution in the form of $P_1(\eta, m)$, $V_1(\eta, m)$ and $R_1(\eta, m)$ respectively, and show that the zero of V_1 is removed unless $m = \frac{2}{3}$ while the zero in density remains. Figure 6 gives the behaviour of the coefficient C_1 as a function of m. The behaviour of V_1 near $\eta = 0$ made it difficult to determine $V_1(0)$ from the computer results, since the calculations had to be stopped short of $\eta = 0$ to avoid the infinite value of some of the derivatives. In order to avoid this difficulty, the independent variable was transformed to $\xi = \eta^{\frac{3}{2}m-1/\gamma}$, and the calculations were repeated with ξ as independent variable, giving a straight line for $V_1(\xi)$ near $\xi = 0$ which could be extrapolated accurately to $\xi = 0$, giving $V_1(0) = m/C_1$ and hence C_1.

The limit cases of the range, $m = \frac{2}{3}$ and $m = \frac{2}{3}/\gamma$, were included in the calculations, and the results obtained earlier are borne out by the behaviour of V_1. When $m = \frac{2}{3}/\gamma$, V_1 has a logarithmic singularity at $\eta = 0$, giving $C_1 = 0$ and when $m = \frac{2}{3}$, $V_1(0) = 0$ giving $C_1 = -\infty$. The three methods of obtaining C_1 afforded by the boundary conditions for V_1 and Y_1 and equation (15) give the same result.

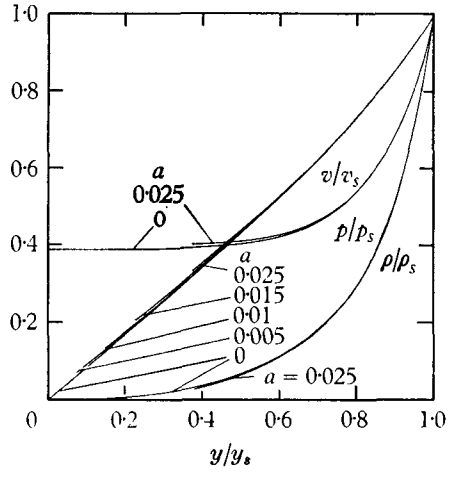

FIGURE 7. Behaviour of the solutions of equations (7) and (8) normalized with respect to values on the shock wave.

$m = \frac{1}{2}$, $a = (C_1/C_0) \times x'^{m-\frac{2}{3}}$, $\gamma = 1·4$.

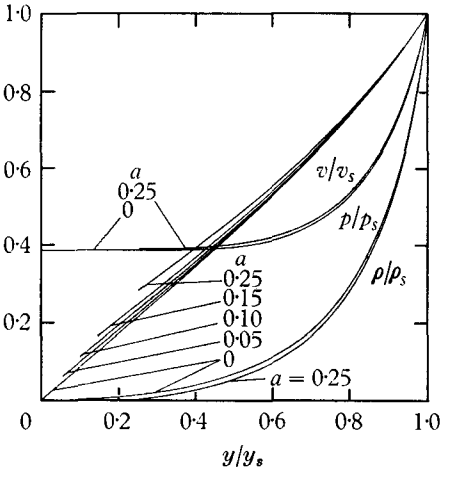

FIGURE 8. Behaviour of the solutions of equations (7) and (8) normalized with respect to values on the shock wave.

$m = \frac{5}{8}$, $a = (C_1/C_0)x'^{m-\frac{2}{3}}$, $\gamma = 1·4$.

Practical implications of theoretical results

The range of x/d for which this analysis can be expected to describe the flow reasonably accurately can now be estimated by requiring that

$$\delta^{1-\frac{3}{2}m}x'^{m-\frac{2}{3}} = (x/d)^{m-\frac{2}{3}} < \epsilon$$

for some small ϵ. The range of validity is then restricted to $x/d > (\epsilon)^{-1/(\frac{2}{3}-m)}$, which for $\epsilon = 0·3$, say, $\gamma = \frac{7}{5}$ and $m = \frac{2}{3}/\gamma$ is about 500. If m is nearer $\frac{2}{3}$, say, for example $m = \frac{5}{8}$, x/d would have to be larger than 3×10^{12}. If this is to be applicable on a body of, say, 50 ft. length, d would have to be smaller than about 10^{-10} in., which is well below the limits of the theory anyway because of restrictions to inviscid and continuum flow. The practical use of the theory is thus clearly

limited. However, it does give an insight into the way in which the blast-wave solution is approached asymptotically and the physical reasons for the deviations from it. The solutions in the outer region have been calculated to second order for $m = \frac{1}{2}$ and $m = \frac{5}{8}$ for various values of $a = (C_1/C_0)(x/d)^{m-\frac{2}{3}}$. They are shown in figures 7 and 8 normalized with respect to values on the shock wave. In shock-normalized co-ordinates the effect of the perturbation is very small in the case of pressure and density, and slightly larger in the case of normal velocity. Pressure and normal velocity are increased while the density is decreased by the perturbation. All these curves have been cut off at the point on the body surface which corresponds approximately to their lower limit of validity in η, that is, where they have to be matched with the inner solution.

3. Experiments at $M_\infty = 8{\cdot}2$

Experimental conditions, models and technique

For an ideal test of the above theory, experiments should be made at very high Mach number and Reynolds number. Both of these conditions could only be satisfied to a limited degree by the available facility and instrumentation. The hypersonic gun tunnel at Imperial College, which has been described in detail by Needham (1963) was used with a contoured nozzle at $M_\infty = 8{\cdot}2$ using air as the test gas. The free-stream stagnation temperature as measured by a thin-wire-resistance thermometer was 665 °K, and the stagnation pressure was 1560 psia. Under these conditions the viscous length scale, ν_∞/U_∞ in the free stream is about 10^{-5} in.

The experiments were made at two values of m in the range $\frac{2}{3}/\gamma < m < \frac{2}{3}$, ($m = \frac{1}{2}$ and $m = \frac{5}{8}$) on plane models. In order to compensate for the great difference in the range of validity of the theory between these two values of m, the length scale d was chosen as $d = 0{\cdot}010$ in. for $m = \frac{5}{8}$ and $d = 0{\cdot}225$ in. for $m = \frac{1}{2}$. The models were 10 in. long and 5 in. wide while the working section of the gun tunnel has a useful core of about 6 in. diameter. Two smaller parabolas ($d = 0{\cdot}100$ in. and $d = 0{\cdot}156$ in.) available from pilot experiments were also tested. The nose of the largest parabola could be replaced by a 30° half-angle wedge which was tangent to the parabola. Figure 19, plate 1, shows the large parabola with traversing gear and Pitot and static probes.

The quantities measured were surface-pressure distribution, shock-wave shape, Pitot pressure, static pressure and streamline slope. The last three of these were measured along lines normal to the body surface at several stations on each model. The static pressure was measured with a probe which was made similar to that reported by Behrens (1963). This consists of a 10° half-angle cone followed by a 1 mm diameter stainless steel tube with 4 pressure holes 15 tube diameters from the cone tip and about 33 tube diameters upstream from the probe support. This probe was calibrated in the shock-layer of a 20° wedge. The reading was found to be insensitive to changes of incidence of $\pm 3°$ which corresponds approximately to the amount by which the streamline slope changes from body to shock wave along lines normal to the body surface. The probe inclination was held constant at the approximate average streamline slope for each traverse. When the static

pressure probe protruded through the shock wave, the interference between probe and shock caused the reading to be unreliable. All such readings were discarded.

The streamline slope was measured by bisecting the angle between two intersecting weak waves. These were generated from strips of adhesive tape 0·0015 in. thick and fixed to the model surface, and from a similar set of adhesive strips

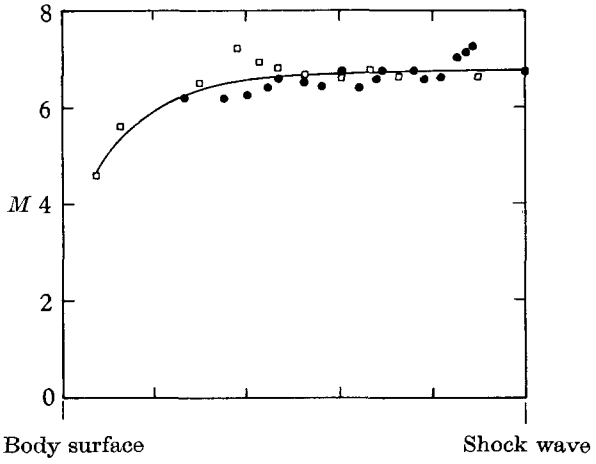

FIGURE 9. Comparison of Mach number as obtained by various methods. $m = \frac{2}{3}$, $x/d = 560$, $d = 0{\cdot}010$ in. ●, method of weak waves; □, static and Pitot pressures; ■, shock-wave slope.

fixed to a sharp flat plate opposite the model and outside the shock wave. Although this method is not very accurate (see figure 9), it gives a large quantity of data in one experimental run and is thus very useful for pilot experiments. The Mach number can also be obtained by this method and this is compared for a particular traverse with the Mach number as obtained from Pitot- and static-pressure measurements in figure 9. The agreement is within an accuracy of $\pm 8\,\%$.

Experimental error

The smallest error in all these measurements was that in the shock-wave shape which was measured from enlarged schlieren photographs to about $\pm 0{\cdot}015$ in. The error in the static-pressure measurements was estimated to be about $\pm 8\,\%$, while that in the Pitot-pressure measurements was about $\pm 5\,\%$. The error in the free-stream stagnation temperature is approximately ± 15 °K, stagnation pressure about $\pm 3\,\%$ while the Mach number is uniform at $8{\cdot}2 \pm 0{\cdot}2$.

4. Experimental results and comparison with theory

Surface pressure distribution

In order to obtain the coefficient C_0 of the first-order quantities, the experimental pressure distributions were integrated numerically to give the drag to x, D_x, as a function of x. The asymptotic drag D_∞ was then obtained by fitting the expression

$$D_x = D_\infty - a(x/d)^{m-\frac{2}{3}}$$

to the experimental curve. An example of such a fit is given in figure 10 for the parabola. D_∞, substituted into equation (14), then gives C_0. Using these values of C_0 all quantities can be obtained from the theoretical results to second order. Although this method gives only an estimate for C_0, it is the result of an integration of experimental quantities and thus likely to be more accurate than the alternative method of comparing the magnitude of first- and second-order quantities directly. It also does not involve the use of any second-order quantities apart from the actual body shape.

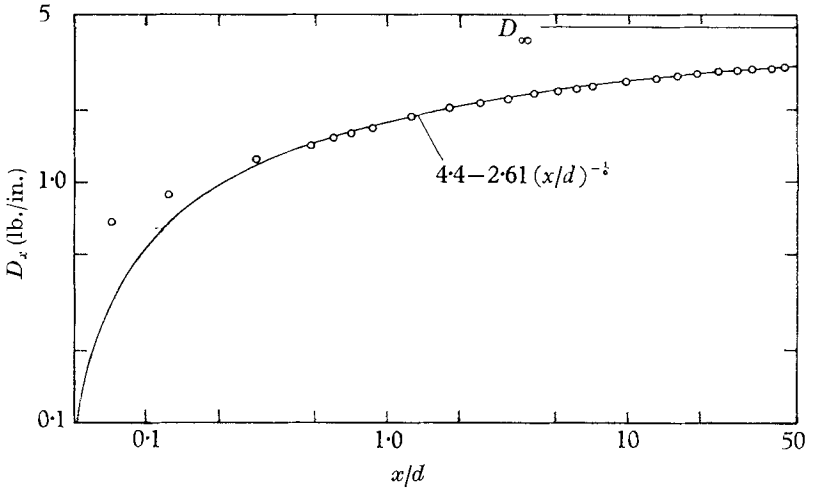

FIGURE 10. Fit of $D_\infty - a(x/d)^{m-\frac{2}{3}}$ to experimental drag, $m = \frac{1}{2}$, $d = 0{\cdot}225$ in., $C_0 = 1{\cdot}4$.

The pressure distributions on the parabola and wedge-parabola (figures 11(*a*) and (*b*)) are seen to be in fair agreement with the present theory, although the effect of finite free-stream pressure manifests itself at large values of x/d. Near the tail end of the model this effect is cancelled again by a fall in pressure which was observed to coincide with the loss of two-dimensionality of the flow. These two effects are best observed in figure 11(*b*), where the experimental pressure distribution for the wedge-parabola is compared also with a characteristics solution by Lewis (1965, unpublished). The deviation from the characteristics solution at large x/d demonstrates the effect of loss of two-dimensionality while the deviation of the second-order theory from the characteristics solution demonstrates the effect of finite free-stream pressure.

In the case $m = \frac{5}{8}$, figure 11(*c*), the weak-shock effect (finite free-stream pressure) is seen to be very strong, and experiment agrees fairly well with the tangent-wedge approximation. However, if this effect is corrected approximately by comparing $p - p_\infty$ with the second-order pressure, the agreement is seen to be quite good. All three experimental pressure distributions show a consistent 'dip' in pressure in the region between $x = 1$ and $x = 3$ in. This has also been observed by Needham (1965) and is associated with a local non-uniformity in the test flow.

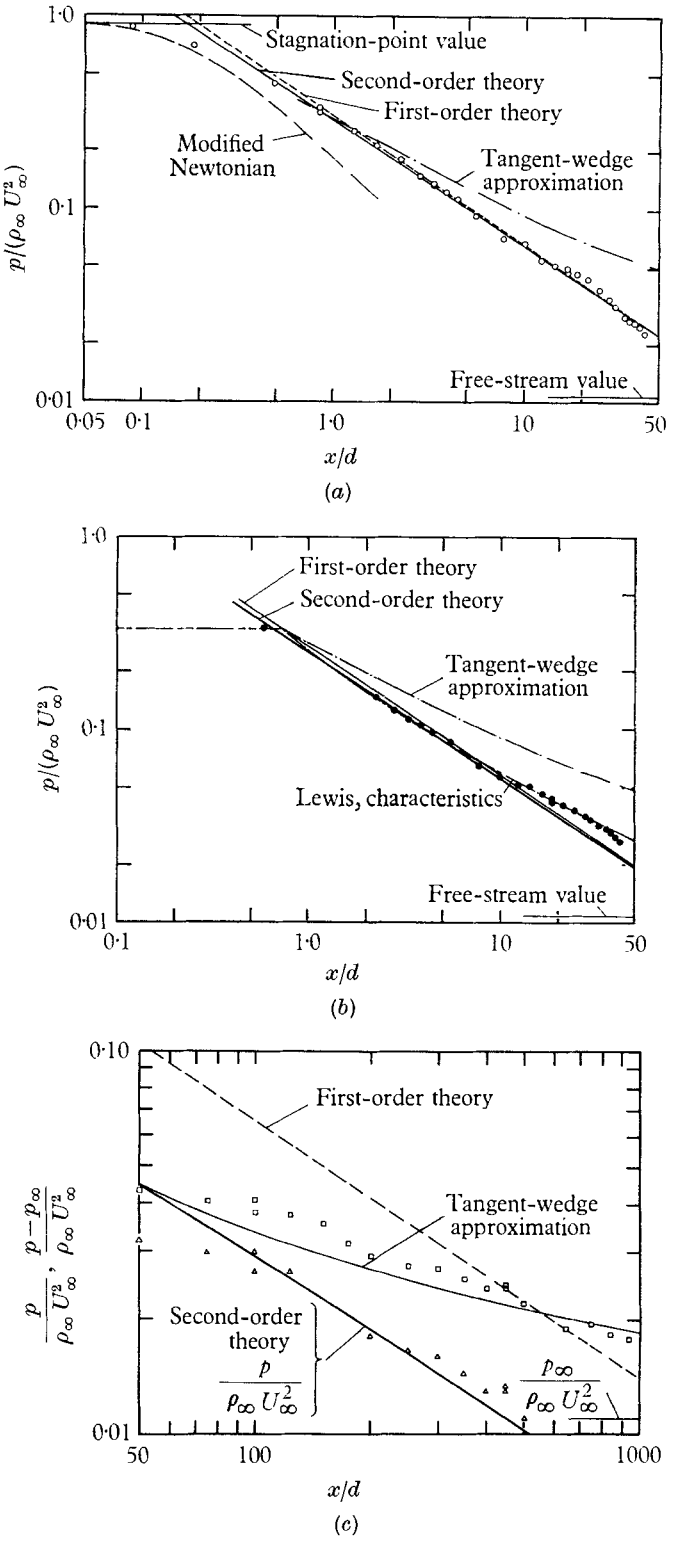

FIGURE 11. (*a*) Surface-pressure distribution on parabola, $m = \frac{1}{2}$, $d = 0{\cdot}225$ in. (*b*) Surface-pressure distribution for a wedge-parabola, $d = 0{\cdot}225$ in., x/d measured from virtual origin of parabolic afterbody. (*c*) Experimental pressure distribution, $m = \frac{5}{8}$, $d = 0{\cdot}010$ in. □, $p/(\rho_\infty U_\infty^2)$; △, $(p-p_\infty)/(\rho_\infty U_\infty^2)$.

Shock-wave shape

The shock-wave shapes as measured on three parabolas with different values of d are plotted in figure 12 (a) as y_s/d versus x/d. It is seen that the shock waves of all parabolas are correlated onto a single curve in these co-ordinates. This was found to be true also for the results of Peckham (1965) and Kubota (1957) for axi-symmetric power-law bodies. It seems reasonable to expect that shock-wave shapes on bodies of the shape $y_b/d = (x/d)^m$ collapse for a particular m onto a single curve in these co-ordinates for large M_∞.

For the other two models the shock-wave shapes are plotted in figures 12 (b) and 12 (c) and compared with the present theory using C_0 as obtained from the drag. As in the pressure distributions, the magnitude of the second-order quantities is seen to be much larger for $m = \frac{5}{8}$ than for $m = \frac{1}{2}$, and the way in which the second-order effect modifies the first-order theory is in the right direction, except in the case of the parabola, where the theoretical prediction for y_s is 10% less than the experimental result. Although a better fit could have been achieved by choosing C_0 and C_1 for fit, this was not done here in order to give a true comparison of theory and experiment.

In the case of the wedge-parabola (figure 12 (b)) a comparison could again be made with the characteristics solution of C. H. Lewis (1965, unpublished) and the agreement is very good. The discrepancy between experiment and characteristics solution at small values of x/d is largely attributable to experimental error amounting to no more than 0·025 in. The shock-wave shapes are shown in the form of schlieren photographs in figures 20 and 21, plate 1.

Shock-layer traverses

Pitot- and static-pressure traverses were made at five stations on the largest parabola ($d = 0{\cdot}225$ in.), three stations on the wedge-parabola, two stations on the $\frac{5}{8}$-power-law body and two stations on the smallest parabola ($d = 0{\cdot}100$ in.). By assuming that the stagnation temperature is constant throughout the flow, all the flow variables can be calculated from these measurements. Figure 13 shows the static-pressure distribution in the shock layer of the parabolas plotted against z/d, where z is the distance normal to the body surface measured from the body surface. The static pressure as measured on the surface of the large parabola at the traverse station is included in figure 13 as a point on the vertical axis. It is seen that this pressure agrees well with the extrapolation of the pressure traverses, giving additional confidence in the static-pressure probe. Although the two-dimensionality of the flow is doubtful on the large parabola for $x/d > 30$, such traverses have been included in figure 13 to show the general trend.

Figure 14 shows the experimental density distribution across the shock layer of the parabolas at various traverse stations. The experimental density and static pressures measured in the shock layer of the $\frac{5}{8}$-power-law model are plotted in figure 15. It is evident from figure 14 that the effect on the density of the weak shock wave is considerable, the density on the shock wave being less than 50% of the value on a strong shock wave for large x/d. It can therefore be expected that the density profiles will not be in good agreement with the theory. This is evident

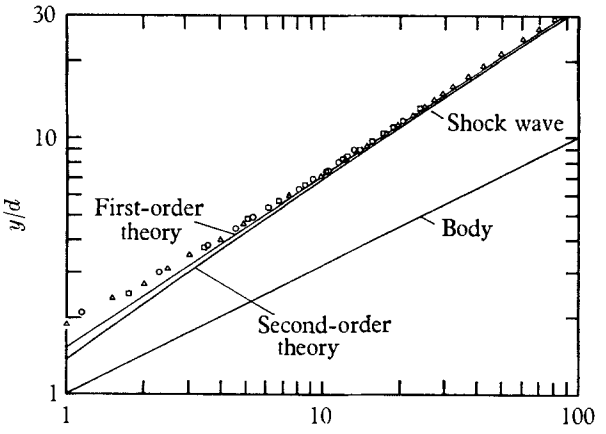

(*a*)

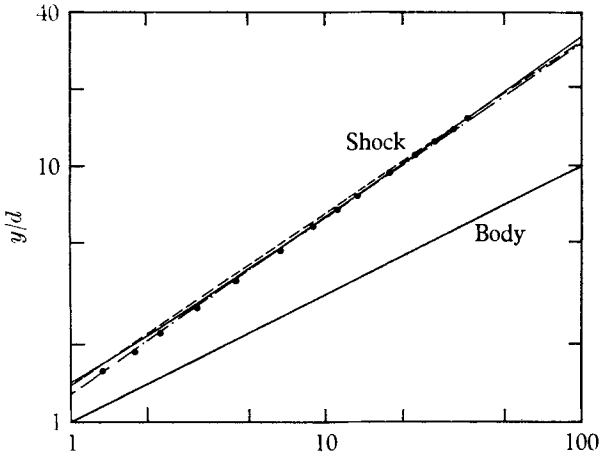

(*b*)

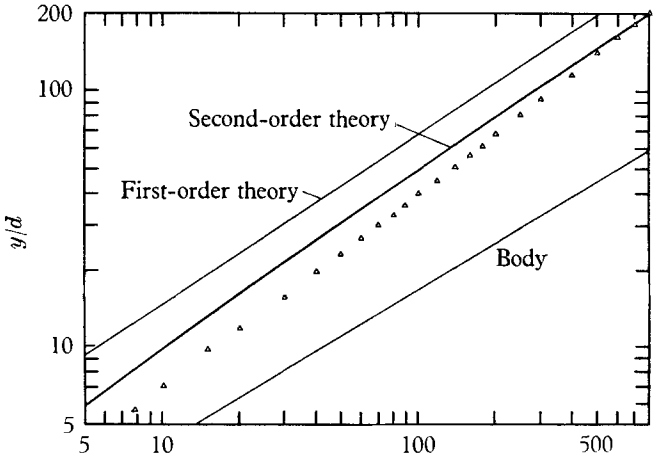

(*c*)

FIGURE 12. (*a*) Shock-wave shape on three plane parabolas. ○, $d = 0{\cdot}225$ in.; □, $d = 0{\cdot}156$ in.; △, $d = 0{\cdot}100$ in. (*b*) Shock-wave shape on wedge-parabola. – – – –, first-order theory; —·—·—, second order theory; ——, characteristics. (*c*) Shock-wave shape, $m = \frac{5}{8}$.

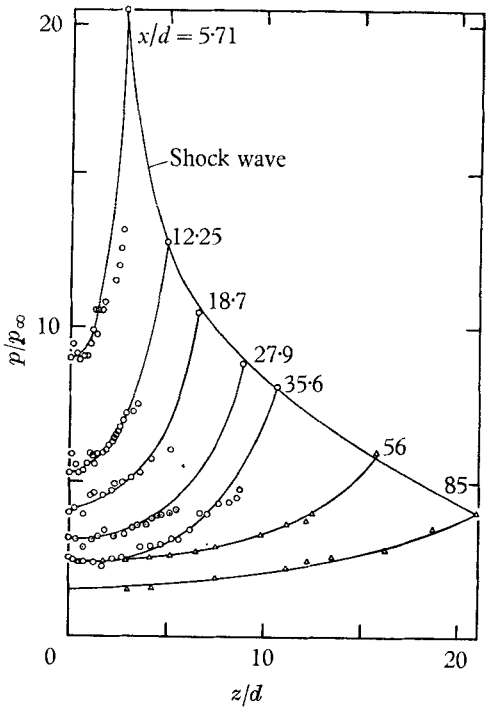

FIGURE 13. Static-pressure distribution through shock layer, $m = \frac{1}{2}$, $p_\infty = 0{\cdot}135$ psia. ——, mean line through experimental points; △, $d = 0{\cdot}100$ in.; ○, $d = 0{\cdot}225$ in.

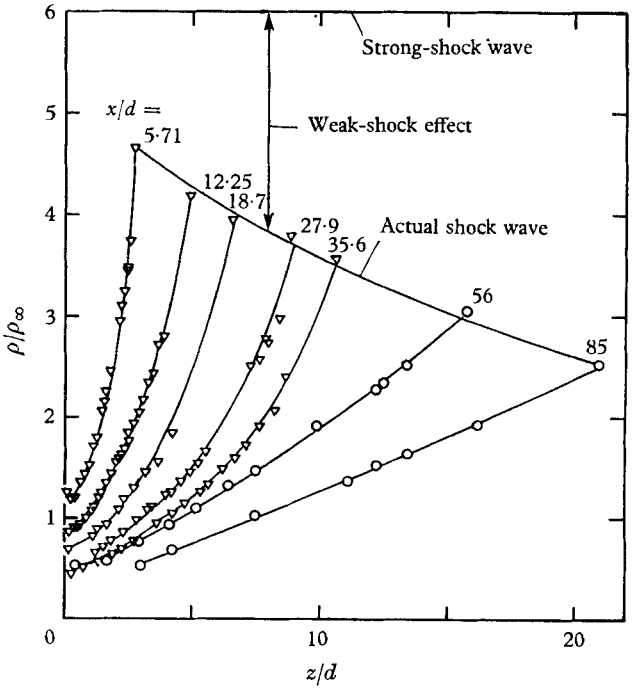

FIGURE 14. Experimental density distribution through shock layer, $m = \frac{1}{2}$, ——, mean line through experimental points; ▽, $d = 0{\cdot}225$ in.; ○, $d = 0{\cdot}100$ in.

even from a cursory inspection of the density profiles for $m = \frac{5}{8}$, whose shape is considerably different from the density profile of figure 8. The general shape of the density profiles on the parabola, however, is similar to the theoretical prediction.

The strong-shock-wave assumption is not so serious in the case of pressure and velocity, and in the hope that the effect of the error in density on these quantities is not too strong, the pressure and normal velocity were compared with theory in figures 16 and 17. The normal velocity v was calculated from the streamline

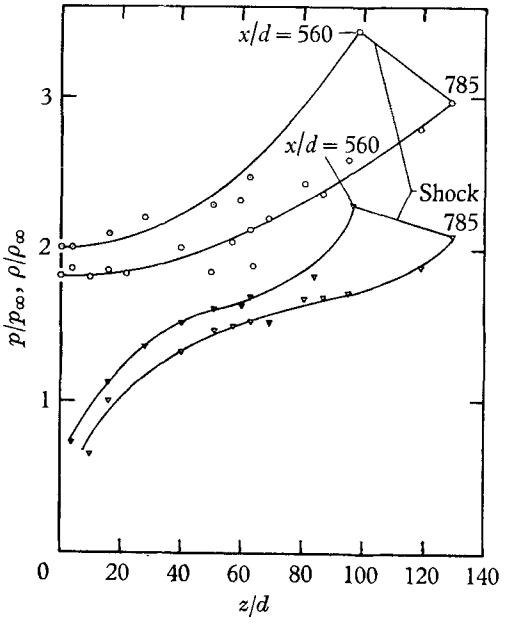

FIGURE 15. Experimental static-pressure and density distributions through shock layer, $m = \frac{5}{8}$. ——, Mean line through experimental points; ○, pressure, p/p_∞; ▽, density, ρ/ρ_∞.

slope and local velocity which were obtained by the method of weak waves and from the pressure measurements respectively. It is seen that in both cases the experimental results for the parabola are in very good agreement with theory. In the case $m = \frac{5}{8}$ the pressure distribution is of the right general shape, but considerably higher than the theoretical prediction. The weak-shock effect (finite free-stream pressure) would account for some of this discrepancy. The normal velocity for $m = \frac{5}{8}$ is also under-estimated by the theory.

An attempt to fit the present theory to the present experimental results for $m = \frac{5}{8}$ must, however, be expected to meet with marginal success only, since the theory requires a value of $x/d > 500$ for convergence, and the shock wave is already very weak at $x/d = 560$.

Figure 18 shows the results of one of the shock-layer traverses on the wedge-parabola in comparison with the characteristics solution of C. H. Lewis (1965, unpublished) at the same station. Except for a deficiency in static pressure of about 8%, which is probably attributable to lack of two-dimensionality at this station ($x/d = 36$), the agreement is seen to be very good.

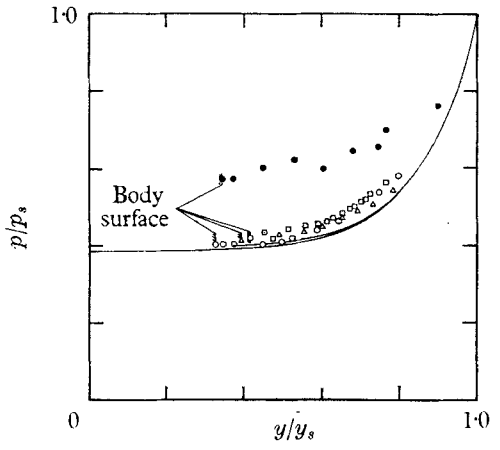

FIGURE 16

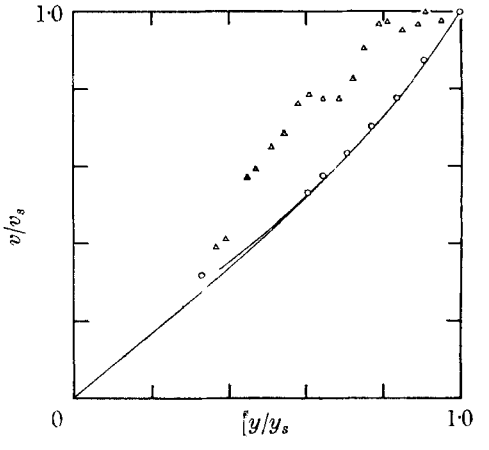

FIGURE 17

FIGURE 16. Pressure distribution through shock layer, comparison with theory. Experiment: □, $x/d = 12{\cdot}25$, $m = 0{\cdot}5$; △, $x/d = 18{\cdot}7$, $m = 0{\cdot}5$; ○, $x/d = 56$, $m = 0{\cdot}5$; ●, $x/d = 560$, $m = 0{\cdot}625$. Theory: $x/d = \infty$ and $x/d = 50$, $m = 0{\cdot}5$.

FIGURE 17. Normal velocity distribution through shock layer, comparison with theory. Experiment: △, $m = 0{\cdot}625$, $x/d = 560$; ○, $m = 0{\cdot}5$, $x/d = 56$. Theory: $x/d = \infty$ and $x/d = 50$, $m = 0{\cdot}5$.

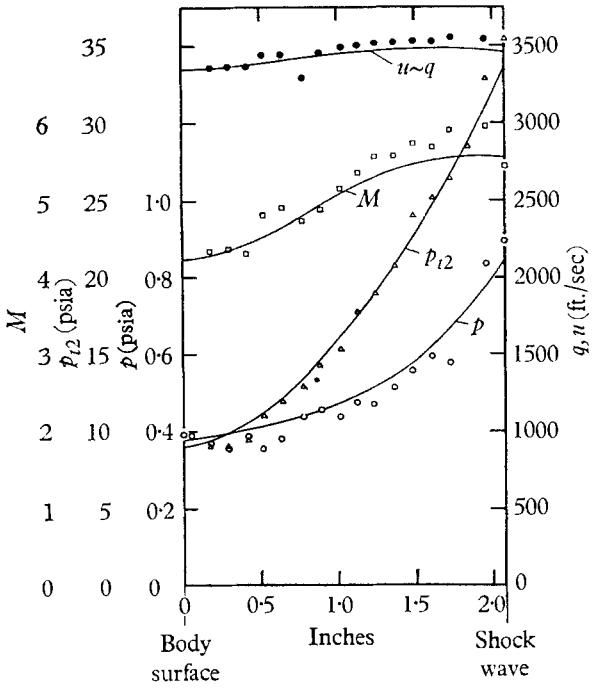

FIGURE 18. Shock-layer traverse, wedge-parabola, $x/d = 36$; comparison with characteristics solution. Experiment: ○, measured static pressure, p; △, measured Pitot pressure, p_{t_2}; ●, derived velocity, q; □, derived Mach number, M; ——, method of characteristics (Lewis 1965, unpublished).

5. Conclusions

Theoretical solutions, based on the expansion scheme for large x and large M_∞ as proposed by Freeman (1962), were obtained for the asymptotic inviscid flow over plane bodies of the shape $y/d = (x/d)^m$ in the range $\frac{2}{3}/\gamma < m < \frac{2}{3}$. These second-order solutions enabled the condition that the body surface be a streamline to be satisfied.

The magnitude of the second-order term was found to increase from zero at $m = \frac{2}{3}/\gamma$ to infinity at $m = \frac{2}{3}$. At these two points it is probably necessary to adopt a more sophisticated approach since, at $m = \frac{2}{3}/\gamma$, a matching condition cannot be satisfied, and at $m = \frac{2}{3}$ the expansion does not converge.

A comparison of experimental shock-wave shapes on plane parabolas of different length scales showed that the significant length scale of the shock-wave shape is the same as that for the body, the shock waves for all parabolas collapsing onto a single curve in the body co-ordinates $y/d, x/d$. The same was found to apply to the axisymmetric power-law bodies of Kubota (1957) and Peckham (1965).

The deviation of the experimental results from first-order theory was generally in the same direction as predicted by second-order theory and the magnitude of the deviation was much larger at $m = \frac{5}{8}$ than at $m = \frac{1}{2}$. This is in agreement with the theoretical prediction. The accuracy of the experimental results was insufficient for a conclusive comparison of the shape of the deviations with the second-order quantities.

The extent of the range of validity of the theory varies with m. An estimate of the range of validity taking $C_0/C_1 = 1$ is pessimistic since the experimental determination of C_0 shows that this ratio is smaller than one. The lower limit of the range of validity appears to be about $x/d = 10$ for $m = \frac{1}{2}$ and $x/d = 500$ for $m = \frac{5}{8}$. These are experimentally feasible conditions although the Mach number in the present experiments was too low for a good comparison in the case $m = \frac{5}{8}$.

A comparison of the experimental results with a characteristics solution for the wedge-parabola confirms the utility of the gun tunnel as a facility for making aerodynamic measurements in steady flows. It also shows that characteristics solutions could be used with confidence as a test of the theory for values of x/d outside the range of experimental facilities.

This work is part of a Ph.D. thesis and was done at the Aeronautics Department of Imperial College. I would like to thank Dr N. C. Freeman for his help and guidance in the theoretical part of the work. I am also very grateful to Mr J. L. Stollery who supervised the project and to Dr C. H. Lewis of the Arnold Engineering Development Center, who supplied the characteristics solution. The Australian Department of Supply gave financial assistance, and thanks are due to the Chief Scientist for permission to publish.

REFERENCES

Behrens, W. 1963 *AIAA J.* **1**, 2864.

Cheng, H. K. & Pallone, A. J. 1956 *J. Aero. Sci.* **23**, 700.

Freeman, N. C. 1962 *NPL Aero Rep.* no. 1035, *ARC* 23999. (See also *Research Frontiers in Fluid Dynamics*, ed. R. Seeger & G. Temple, p. 284. New York: Interscience.)

FREEMAN, N. C., CASH, R. F. & BEDDER, D. 1964. *J. Fluid Mech.* **18**, 379.

GOLDSWORTHY, F. A. 1952 *Quart. J. Mech. Appl. Math.* **5**, 54.

GUIRAUD, J. P. 1958 *C.R. Acad. Sci., Paris*, **246**, 2842.

GUIRAUD, J. P. 1964 *Int. Symp. on Fund. Phenomena in Hyp. Flow.* Buffalo: Cornell University. (Also *ONERA* T.P. 132.)

GUIRAUD, J. P., VALLÉE, D. & ZOLVER, R. 1965 *Basic Developments in Fluid Dynamics*, ed. M. Holt, vol. I, p. 127. New York: Academic Press.

HAMMITT, A. G. & BOGDONOFF, S. M. 1956 *Jet Propulsion*, **26**, 241.

HAYES, W. D. 1947 *Quart. Appl. Math.* **5**, 105.

KUBOTA, T. 1957 *GALCIT Memo.* no. 40.

LEES, L. & KUBOTA, T. 1957 *J. Aero. Sci.* **24**, 195.

LEES, L. 1955 *Proc. 5th Int. Aero. Conf.*, Los Angeles, p. 241.

MESSITER, A. F. 1965 *BAMIRAC Rep.* no. 4613-81-T.

NEEDHAM, D. A. 1963 *I.C. Dept. of Aeronautics Rept.* no. 118.

NEEDHAM, D. A. 1965 Ph.D. Thesis, London University.

PECKHAM, D. H. 1965 *ARC* 27084.

SEDOV, L. 1959 *Similarity and Dimensional Methods in Mechanics.* English edition ed. M. Holt. New York: Academic Press.

TAYLOR, G. I. 1950 *Proc. Roy. Soc.* A, **201**, 159.

VAGLIO-LAURIN, R. 1964 *Polytech. Inst. Brooklyn Rept.* no. 805.

VAN DYKE, M. D. 1954 *NACA Rept.* no. 1194.

YAKURA, J. K. 1962 Hypersonic Flow Research, ed. F. R. Riddell. *Progress in Astronautics and Rocketry*, vol. 7, p. 421. New York: Academic Press.

ZOLVER, R. 1964 *C.R. Acad. Sci., Paris*, **258**, 5152.

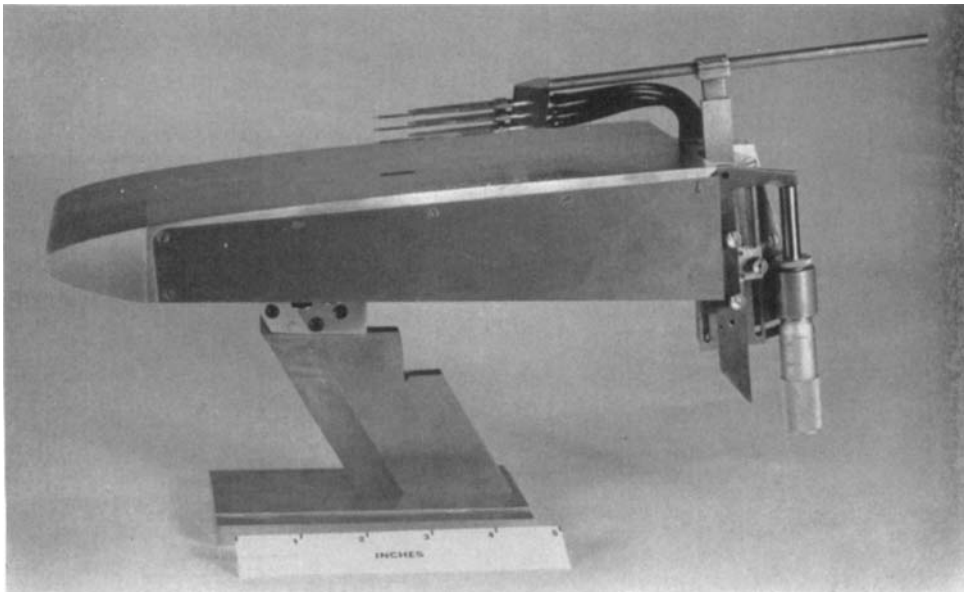

FIGURE 19. Large parabola (d = 0·225 in.) mounted on sting, showing traverse mechanism and probes.

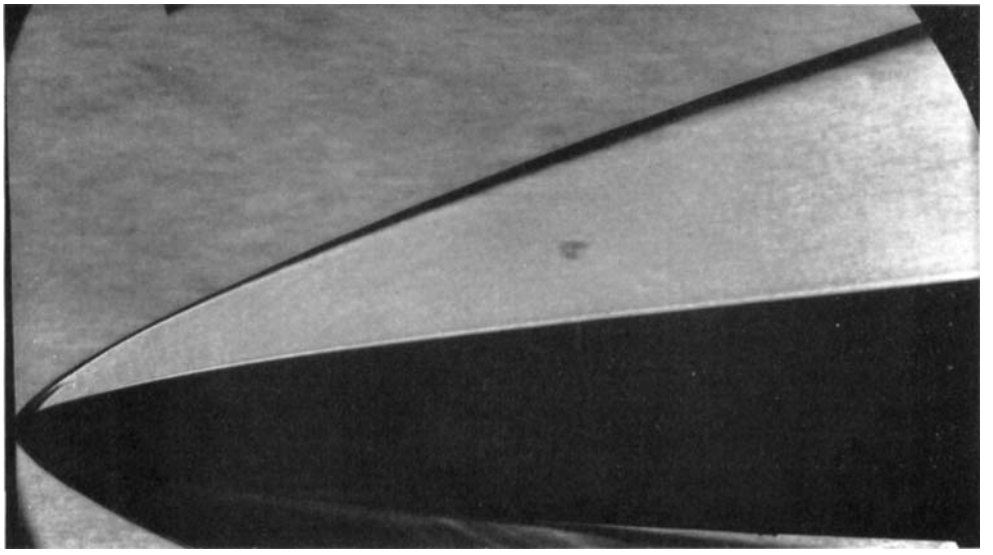

FIGURE 20. Shock-wave shape on parabola, d = 0·100 in.

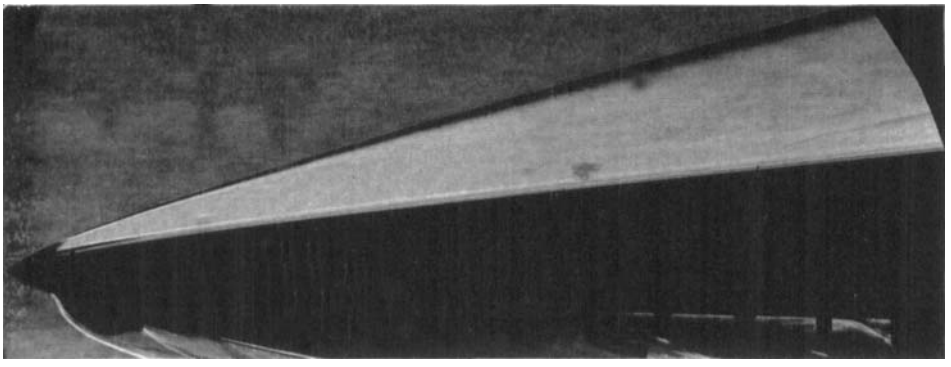

FIGURE 21. Shock-wave shape, $m = \frac{5}{8}$, $d = 0{\cdot}010$ in.